

# Probing nonlinear spin dynamics in canted easy-plane antiferromagnets using spin-rectification effects

A. El Kanj,<sup>1</sup> S. Manton,<sup>1</sup> I. Boventer,<sup>1</sup> P. Bortolotti,<sup>1</sup> V. Cros,<sup>1</sup> A. Anane,<sup>1</sup> O. Gomonay,<sup>2</sup> and R. Lebrun<sup>1</sup>

<sup>1</sup>*Laboratoire Albert Fert, CNRS, Thales, Université Paris-Saclay, 91767 Palaiseau, France*

<sup>2</sup>*Institut für Physik, Johannes Gutenberg-Universität Mainz, Staudingerweg 7, D-55099 Mainz, Germany*

We investigate spin-rectification phenomena in canted antiferromagnets, closely connected to the family of altermagnetic materials. Our results show that excitation efficiency is significantly enhanced by the Dzyaloshinskii-Moriya interaction. Antiferromagnetic dynamics can be detected through spin-Hall magnetoresistance and bolometric effects, with an efficiency reaching up to mV/W. The rectified voltage shape is influenced by both the symmetry of the exciting torques, detection mechanisms (continuous spin-pumping and spin-Hall magnetoresistance), and the antiferromagnetic crystalline axis. Under high pumping power, we observe a saturation effect related to Suhl-like spin-wave instabilities and a nonlinear redshift of the antiferromagnetic resonance. These findings open new avenues for studying nonlinear dynamics in antiferromagnetic and altermagnetic spintronic devices.

Spin dynamics in antiferromagnets (AFMs) and altermagnets offer exciting prospects for spintronic devices operating at frequencies beyond several GHz, reaching into the THz range [1–3]. AFMs also provide access to rich, largely unexplored physics, such as inertial spin dynamics [4], eigenmodes with noncircular polarization [5], nonlinear dynamics between eigenmodes [6, 7], and superfluid states [8]. However, the vanishing net magnetic moment, combined with exchange-enhanced linewidths, complicates the detection and control of AFM magnetization dynamics using conventional electronic methods. In contrast, altermagnets [9], and the closely related family of canted antiferromagnets [7], inherit the ultra-fast AFM responses and the presence of small net magnetization in their AFM domains or domain walls however enables an easier control of AFM domains by external magnetic fields and magnetic field gradients [10]. To date, magnonic studies in antiferromagnets have primarily focused on uniform oscillations [11], with only recent reports of spin-wave dynamics in single crystals [12–14]. In parallel, the advent of high-power femtosecond lasers has enabled the first observations of nonlinear uniform spin-excitations in antiferromagnets [7, 15–17]. Spintronic-based approaches for electrically accessing and detecting AFM spin dynamics have also been proposed. [18–20].

In ferromagnets, spin-dynamics are commonly detected via spin-diode effects, in which injected microwave currents are rectified through magnetoresistive oscillations or spin-pumping-induced continuous voltages [21]. The shape of the rectified voltage depends on the type of excitation (e.g., spin torques or current driven-fields) and the detection mechanism (e.g, spin-pumping or spin-Hall magnetoresistance) [22, 23]. An alternative bolometric detection method, using an adjacent platinum thermal sensing layer, is also possible [24]. These rectification mechanisms could similarly be applied to study AFM spin dynamics. However, spin-diode phenomena in antiferromagnets have been theoretically explored in collinear AFMs for spin-orbit torque ex-

citation [20, 25], and lacks of experimental evidence, aside from coupled dynamics between ferromagnets and AFMs [26]. Theoretically, detection efficiencies as large as mV/mW can be anticipated [20], which surpass standard inverse spin-Hall measurements by several order of magnitudes [27, 28]. In microstrip geometries with a small cross-sectional area, the generation of strong microwave fields near the platinum detecting interface could enable the study of nonlinear AFM spin dynamics. At high excitation powers, this approach could extend the study of Suhl instability concepts—originally developed for ferromagnets, involving coupling between  $k = 0$  and  $k \neq 0$  modes—to antiferromagnetic materials [29–32]. Canted antiferromagnets and altermagnets on the other hand, thanks to their non-compensated spin-dynamics [10], offer the ideal playground to access electrically spin diode effects and nonlinear AFM spin dynamics.

In this article, we demonstrate spindiode and bolometric detection of antiferromagnetic resonance in both linear and nonlinear regimes using bilayers of the canted easy-plane antiferromagnet  $\alpha$ -Fe<sub>2</sub>O<sub>3</sub> and a heavy metal. By combining experiments with analytical models, we identify contributions to the rectified voltage from spin-Hall magnetoresistance and spin-pumping, revealing that the shape of the rectified voltage is strongly dependent on the orientation of the antiferromagnetic crystalline axis. Additionally, we show that detection efficiency can be enhanced by a continuous current through bolometric detection of the antiferromagnetic resonance in the heavy metal. At low power, we measure a spin-rectified voltage with a record efficiency of 1 mV/W, comparable to that of ferromagnets, attributed to the large spin-Hall magnetoresistance [33, 34]. At higher pumping power, we observe the onset of a spin-wave instability, resulting in linewidth broadening and saturation of the rectified voltage.

We first investigate antiferromagnetic spin-rectification by injecting a resonant radiofrequency current into a 5 nm thick platinum stripe deposited

on *c*-plane oriented single crystals of  $\alpha$ - $Fe_2O_3$  in the canted easy-plane AFM phase (see Fig. 1a). At the AFM resonance, we successfully detect a rectified continuous voltage in the microvolt range using a lock-in amplifier, which is approximately two orders of magnitude larger than the inverse spin-Hall signal measured at similar input power [27, 28]. As shown in Fig. 1.b, the frequency dependence of the rectified voltage aligns with the dispersion relation of the low-frequency mode of hematite [11, 27]. While the amplitude of the rectified voltage is comparable to that of a similar device patterned on a 1  $\mu$ m thick YIG film, its shape is notably asymmetric, showing a pronounced anti-symmetry with respect to the resonance field. Additionally, the sign of the rectified voltage is opposite for  $\alpha$ - $Fe_2O_3$  compared to YIG. As shown in Fig. 1.c, we also observe that the sign of the rectified voltage reverses with the opposite direction of the applied magnetic field, consistent with spindiode phenomena [21]. In Fig. 1.d, we present the angular dependence of the rectified voltage, revealing  $\pi$  periodic oscillations that reach their maximum when the magnetic field is applied at  $45^\circ$  relative to the direction of the injected RF current. These two features (the angular dependence and the anti-symmetric shape) differ from those observed in antiferromagnetic spin-pumping measurements [35, 36].

To analyze the origin of this rectified voltage, we develop an analytical model based on the approach by Chiba et al. for ferromagnets [21]. We first derive the expressions for magnetization dynamics in the presence of both Oersted field and spin-torque excitation (see Supplementary [37] for details):

$$\begin{aligned} & \mathbf{n} \times [\ddot{\mathbf{n}} + \Delta\omega\dot{\mathbf{n}} - \gamma^2 H_{\text{ex}} \mathbf{H}_{\mathbf{n}}] = \\ & = \gamma^2 H_{\text{DMI}} (\hat{z} \times \mathbf{n}) \times \mathbf{h}(I(t)) - \gamma^2 H_{\text{ex}} \Lambda \mathbf{n} \times [\mathbf{n} \times \boldsymbol{\mu}_0(I(t))] \\ & - \gamma \mathbf{n} \times [\dot{\mathbf{h}}(J(t)) - \Lambda \mathbf{n} \times \boldsymbol{\mu}_0(J(t))] \times \mathbf{n}. \end{aligned} \quad (1)$$

Here  $\mathbf{n} = (\mathbf{M}_1 - \mathbf{M}_2)/M_s$  is the Néel vector ( $|\mathbf{M}_1| = |\mathbf{M}_2| = M_s$ ),  $\mathbf{H}_n$  is the effective anisotropy field,  $\gamma$  is the gyromagnetic ratio,  $\Delta\omega$  is the linewidth (inverse relaxation time).  $H_{\text{ex}}$  is the intersublattice exchange field, while the DMI field  $H_{\text{DMI}}$  is responsible for small canted moment  $\mathbf{m}_0 = H_{\text{DMI}} (\hat{z} \times \mathbf{n}) / H_{\text{ex}}$  in equilibrium state. Vectors  $\boldsymbol{\mu}_0$  and  $\mathbf{h}(t)$  respectively describe the spin accumulation at the Pt interface and the ac magnetic field generated by the ac current  $J(t)$ . Formally,  $\mathbf{h}(t)$  also includes a spin-accumulation contribution (field like torque), proportional to the imaginary spin-mixing conductance  $G_i$ , which is negligible in spin-Hall magnetoresistance measurements [33, 34]. Spin-pumping and spin-torque contributions are characterised by the constant

$$\Lambda = \frac{G_r}{4e^2 M_s d_{\text{AF}} [1 + 2\lambda\rho G_r \coth \frac{d_N}{\lambda}]}$$

which depends on the real spin-mixing conductance  $G_r$ , the electron charge  $e$ , the spin diffusion length  $\lambda$ , the

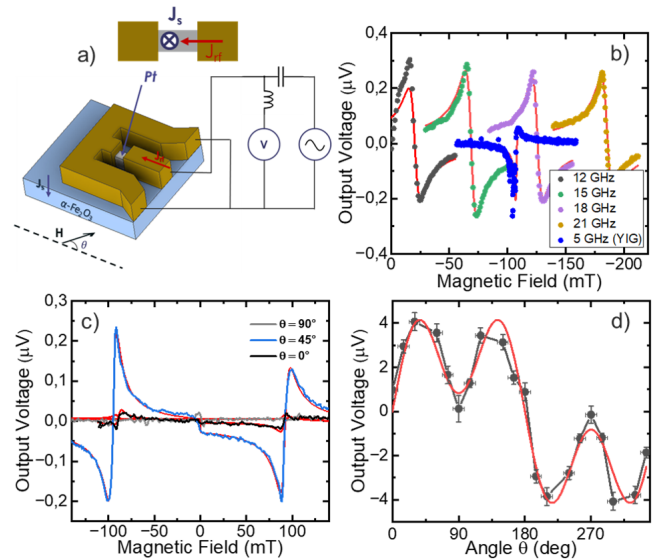


Figure 1. Spin-rectification in 10  $\mu$ m wide stripes of bilayers of the canted antiferromagnet  $\alpha$ - $Fe_2O_3$  (with *c*-plane orientation) capped with 5 nm of platinum. (a) Sketch of the experimental devices. The radiofrequency excitation and detection are respectively performed through a bias-tee by a microwave source (1-22 GHz) and by a lock-in amplifier. An external magnetic field is applied at angle  $\theta$  from the direction of the platinum stripes. (b) Spin-rectification for different exciting frequencies at  $\theta = 45^\circ$ . (c) Exemplary spectra for  $\theta = 0^\circ$ ,  $45^\circ$  and  $90^\circ$  at 17 GHz. The small asymmetry arises from nonfully saturated states when sweeping from negative to positive magnetic field. (d) Angular dependency of the rectified voltage. Red line shows the expected theoretical dependencies from Eq. (2).

(1) Pt resistivity  $\rho$ , and the thicknesses of Pt  $d_N$  and of the antiferromagnet  $d_{\text{AF}}$ . While these spin-torque contributions become negligible in the limit of a thick antiferromagnetic layer  $d_{\text{AF}} \rightarrow \infty$ , where  $\Lambda \rightarrow 0$ , they can be significant in thin films. Notably, the first two terms on the right-hand side of Eq. (1) describe the current driven ac field and anti-damping torques similar to those in FMs, while the third and fourth terms are specific to AFM and play an important role in the presence of an ac field that we will discuss later.

The generated antiferromagnetic spin dynamics produces a spin current that propagates toward the heavy metal, leading to a continuous voltage through both spin-pumping and the rectification of spin-Hall magnetoresistance (SMR) oscillations. The contributions can be expressed as  $V_{\text{SMR}} \propto [n_{0y} \langle J_c^{(0)}(t) \delta n_y \rangle + m_{0y} \langle J_c^{(0)}(t) \delta m_y \rangle]$  and  $V_{\text{SP}} \propto \langle [\delta \mathbf{n} \times \dot{\delta \mathbf{n}} + \delta \mathbf{m} \times \dot{\delta \mathbf{m}}] \cdot \hat{y} \rangle$ . Note that there are two contributions in  $V_{\text{SMR}}$ , however, the second one (which is proportional to magnetization) is substantially smaller (as confirmed by the negative sign of the SMR in AFMs as hematite [33, 34]) and can be neglected. Similarly, in  $V_{\text{SP}}$ , when the easy-plane and the sample

plane coincides as in *c*-cut hematite, the oscillating term of the low frequency mode proportional to the Néel vector leads to out-plane spin-accumulation and can thus be disregarded. We then derive the expressions for the rectified voltage generated at resonance by both  $V_{\text{SMR}}$  and  $V_{\text{SP}}$  (see Supplementary [37] for the details):

$$\begin{aligned} V_{\text{SMR}} &= -\frac{\pi h d_N}{c} \Delta \rho_1 J^2 F(H_0; \omega_{\text{ac}}) \sin 2\theta \cos \theta, \\ V_{\text{SP}} &= \frac{4\pi \hbar \theta_{\text{SH}}}{ec \Delta \rho_0} \frac{H_{\text{DMI}} \omega_{\text{ac}}^2}{H_{\text{ex}}} F(H_0; \omega_{\text{ac}}) V_{\text{SMR}}, \end{aligned} \quad (2)$$

where the line shape is defined by the function

$$F(H_0; \omega_{\text{ac}}) = \frac{\gamma(H_0 - H_r) + \delta \Delta \omega \omega_{\text{ac}} / \gamma H_{\text{DMI}}}{\gamma^2 (H_0 - H_r)^2 + \Delta \omega^2 (\omega_{\text{ac}} / \gamma H_{\text{DMI}})^2} \quad (3)$$

Here  $H_r$  is the resonance field [27],  $h$  is the length of the Hall bar,  $c$  is the speed of light,  $\theta_{\text{SH}}$  is the Pt spin-Hall angle,  $\omega_{\text{ac}}$  is the ac current frequency,  $\hbar$  is the Planck constant.  $\Delta \rho_0$  and  $\Delta \rho_1$  are the conventional SMR resistivities as introduced in [38], and  $\delta = \frac{\Delta \lambda \theta_{\text{SH}} \rho_{\text{ce}}}{\pi \gamma H_{\text{DMI}}} \tanh \frac{d_N}{2\lambda} / d_N$  a prefactor normalizing the Oersted field induced torque and the anti-damping torque (respectively the first and second terms in Eq. (1)). As mentioned above,  $\delta \propto 1/d_{\text{AF}}$  so that the interfacial contributions (symmetric in shape) from the current induced spin-torque can be neglected for thick films ( $> 30 - 50$  nm). The bulk contributions generated by the Oersted field in  $V_{\text{SP}}$  and  $V_{\text{SMR}}$  exhibit the same  $\pi$  periodic angular dependence (see Eq. 2) but  $V_{\text{SP}}$  is symmetric whilst  $V_{\text{SMR}}$  is anti-symmetric. In *c*-cut samples, the measured spin-rectified voltage is anti-symmetric (Fig. 1b-c), indicating that it mainly arises from the rectification of the injected radiofrequency current combined with oscillations of the spin-Hall magnetoresistance. This observation is also in line with the large spin-Hall magneto-resistance ratio of hematite [33, 34]. However, the situation could differ for other crystallographic orientations, when the AFM easy-plane and the sample plane are not aligned. In these cases, the Oersted contribution includes a non-zero out-of-plane component, which also excites the Néel vector dynamics (see last term of Eq. (1)).

To investigate the impact of the cut orientation on the rectified voltage, we examine devices fabricated on a R-plane oriented crystal of hematite, where the easy plane is tilted at  $\psi = 33^\circ$  from the sample surface. In Fig. 2, we present the rectified voltage at 17 GHz in a device oriented at  $45^\circ$  from the in-plane axis of the easy plane [37] for different magnetic fields applied in the device plane. We observe that the shape of the rectified voltage is no longer purely anti-symmetric and varies with the direction of the applied fields. As shown in Fig. 2b-c, the angular dependence exhibits a maximum in amplitude around  $\theta=0^\circ$  and a maximum around  $90^\circ$ , shifted by  $45^\circ$  compared to *c*-plane orientation, and a minimum in resonance field at  $45^\circ$  which belongs to the

easy-plane. According to Eq. (2), a symmetric contribution to the rectified voltage can only arise from the presence of an anti-damping torque, which is not expected for thicknesses exceeding 50 nm.

To explain this discrepancy, we extend our modeling approach for arbitrary easy-plane orientation. We derive the revised expressions for the continuous spin-pumping and spin-Hall magnetoresistance voltages, focusing here solely on the contributions from the Oersted field:

$$\begin{aligned} V_{\text{SMR}} &= -\frac{\pi h d_N}{2c} \Delta \rho_1 J^2 \frac{\sin 2\theta F(H_r^{\text{R}}, \delta_{\text{SMR}}) \cos^3 \psi}{1 - \sin^2 \psi \sin^2 \theta} \\ V_{\text{SP}} &= -\frac{4\pi^2 \hbar \theta_{\text{SH}} \Delta \rho_1 h d_N}{ec^2 \Delta \rho_0} J^2 (H_r^{\text{R}}, \delta_{\text{SP}}) \sin^2 \psi \end{aligned} \quad (4)$$

where  $F(H_r, \delta_{\text{SMR}}, \omega_{\text{ac}})$  are defined in Eq.(3) with the angular-dependent resonant field

$$H_r^{\text{R}} = \frac{H_r^{\text{c}}}{\sqrt{1 - \sin^2 \psi \sin^2 \theta}}, \quad (5)$$

and the symmetric prefactors:

$$\delta_{\text{SMR}} = \frac{\omega_{\text{ac}} \tan \psi}{\gamma H_{\text{DMI}} \cos \theta} \sqrt{1 - \sin^2 \psi \sin^2 \theta}, \quad \delta_{\text{SP}} = 0. \quad (6)$$

Here  $H_r^{\text{c}}$  is the resonant field at a given frequency for *c*-cut.

Noteworthy, Eq. (4) predicts different angular dependencies for the  $V_{\text{SMR}}$  and  $V_{\text{SP}}$  contributions. The  $V_{\text{SP}}$  contribution is completely anti-symmetric ( $\delta_{\text{SP}} = 0$ ), while the symmetry of the  $V_{\text{SMR}}$  contribution varies with  $\theta$ , allowing it to have a symmetric shape even in the absence of anti-damping torque. Unlike in ferromagnets [21], the presence of a sizeable contribution from anti-damping torque cannot be inferred solely from the

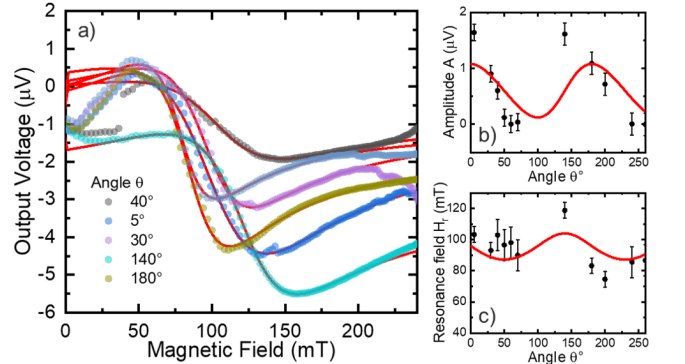


Figure 2. Spin-rectification at 17 GHz in 10  $\mu\text{m}$  wide stripes of bilayers of the canted antiferromagnet  $\alpha\text{-Fe}_2\text{O}_3$  (with R-plane orientation) capped with 5 nm of platinum. (a) Exemplary spectra for different  $\theta$  angles. (b-c) Inplane angular dependency of the resonance field and peak-peak voltage on the applied magnetic field. Solid red lines show the theoretical dependencies calculated according to Eqs. (4) and (5).

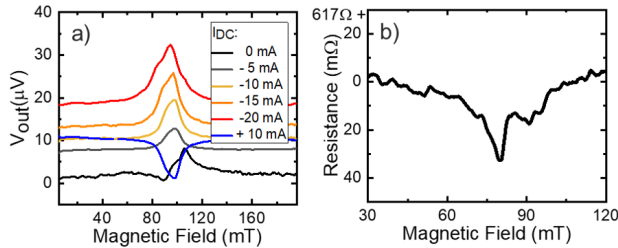


Figure 3. Bolometric detection of the AFM resonance (a) Rectified voltage as a function of the applied DC current for a fixed RF power of 3 mW in a 2  $\mu\text{m}$  wide device. (b) Resistance change in the platinum stripe at resonance for a RF power of 10 mW.

voltage shape. By fitting the experimental angular dependence (see Fig. 2c) with Eq. (4), we find that  $V_{SMR}$  contributes the most to the signal, even for R-plane samples. The amplitude of the rectified voltage remains in the microvolt range for both orientations, similar to that observed in ferromagnets. This aligns with the SMR ratio, which is also on the order of  $10^{-4}$  in both insulating AFMs [33, 34, 39] and FMs [40, 41], resulting in comparable detection efficiencies [25].

We then explore if a continuous (dc) current could modify the spin-rectified voltage even in the case of a bulk AFM crystal. In the simpler case of c-plane orientation (see Fig. 1a), the shape of the spin-rectified voltages, shown in Fig. 3a, progressively changes from antisymmetric to symmetric when increasing the current from 0 to +20 mA. This change might appear as a signature of the presence of spin-torque phenomena at the antiferromagnet/heavy metal interface, as indicated by Eq. (2). Notably, we detect a linear increase in voltage with applied dc current, although we do not expect significant spin-orbit torque contributions in micrometer-thick single crystals. However, we also find that the rectified voltage reverses for negative current, which is thus indicative of bolometric detection [24], linked to a temperature rise in the Pt from energy dissipation at antiferromagnetic resonance. To confirm this observation, we measure the resistance of the platinum stripes during resonance excitation, finding a change of about 20 m $\Omega$  at 10 mW (see Fig. 3b), corresponding to a temperature increase of roughly 30 K. Thus, we can enhance the detected voltage by increasing the applied dc current. For instance, we achieve in Fig. 3a a rectified voltage exceeding 20  $\mu\text{V}$  at 10 mW with a 20 mA DC current, resulting in an efficiency of 1 mV/W. Using more resistive, for example by narrowing the platinum stripes, we anticipate to be able to reach voltages up to several millivolts. This makes this approach promising for detecting sub-THz signals in other insulating antiferromagnets, with limitations only related to thermal response times (tens of kHz) and the absence of phase resolution.

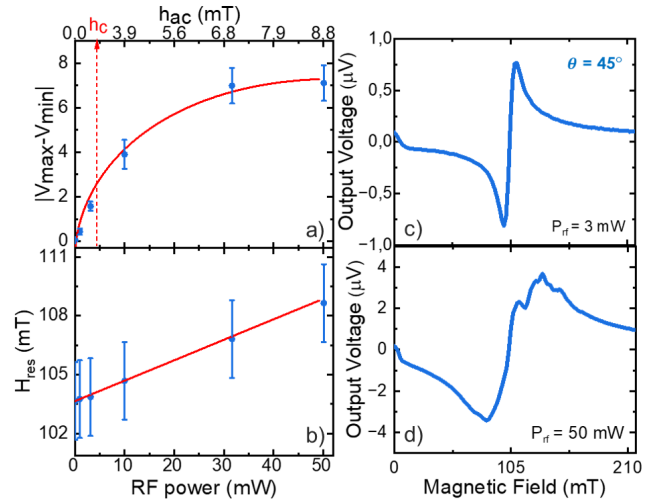


Figure 4. Power dependency of the rectified voltage for a fixed input frequency of 17 GHz in a 10  $\mu\text{m}$  wide device at  $\theta = 45^\circ$ . Amplitude (a) and resonance frequency (b) of the rectified voltage with the power of the injected RF current. Red lines corresponds to the theoretical response including nonlinear spin-wave excitation. (c-d) Exemplary spectra at 5 and 17 dBm, showing the onset of a nonlinear behaviour

To finally gain further insights into the magnetization dynamics of the antiferromagnet, we record the rectified voltage for varying input RF power (without dc current). As shown in Fig. 4, we observe a linear increase in the rectified voltage up to 31 mW (15 dBm), peaking at around 7  $\mu\text{V}$ . We also observe that the resonance frequency shifts from 105 to 110 mT. This nonlinear frequency shift arises from large amplitude of uniform oscillations, characterized by a reduction of the averaged Néel vector and consequently of the effective anisotropy. This reduction leads to an amplitude-dependent resonance frequency, which can be linearized for small excitations  $\omega_{\text{res}} \approx \omega_0(1 - A^2/4)$  (see Fig. 4b), where  $\omega_0(H)$  is the AFM resonance frequency, and  $A$  is the linearized amplitude of the oscillations,  $A \approx \gamma^2 H_{\text{DMI}} h_{0y} / (4\Delta\omega\omega_0)$ .

Above 15 mW, we detect a saturation of the rectified voltage alongside linewidth broadening. Firstly, the voltage saturation can be associated with a saturation of the oscillation amplitude. The ac field excites both uniform and nonuniform ( $\mathbf{k} \neq 0$ ) oscillations. In the linear regime, the frequency of the nonuniform mode is always higher than that of the uniform mode, and  $A$  increases with  $h_{y0}$ . However, due to nonlinear coupling, the frequency of the nonuniform mode decreases more rapidly than  $\omega_{\text{res}}$ . At a critical value  $h_{0y}^{\text{cr}}$ , both frequencies coincide, resulting in resonant excitation of the nonuniform mode at high amplitude, which absorbs energy from the pumping field, leading to saturation of the uniform mode's amplitude. This process thus corresponds to a multi-magnon process, corresponding in the conversion from uniform to non-uniform spin-



waves mode, and the saturation can be attributed to the Suhl instability [29–31]. It is noteworthy that the DMI-mediated coupling with the magnetic field plays an important role in the observation of the Suhl instability in easy-plane systems. In particular, the effective ac field depends on the DMI value and on the orientation of the magnetic vectors. Its value decreases as the oscillation amplitude increases, leading to a saturation. By adapting Eq. (1) of Ref. [30] to hematite, we thus estimate the critical field for spin-wave instability to be  $h_{0y}^{\text{cr}} \approx (2\Delta\omega)^{3/2}\omega_{\text{res}}^{1/2}/(\gamma^2 H_{\text{DMI}}) \approx 1$  mT which is exceeded for input power of a few mW [37]. For larger excitation fields, both the uniform mode and the spin-wave mode are excited, contributing to a progressive saturation of the oscillation amplitude [37]. Secondly, the significant linewidth broadening observed at high power, can be attributed to the excitation of nonuniformly propagating modes that transfer energy away from the region beneath the Pt electrode. We can rule out linewidth broadening due to a temperature increase, as the Néel temperature of  $\alpha$ -Fe<sub>2</sub>O<sub>3</sub> is approximately 780 K, while the temperature rise in platinum remains below 50 K at 100 mW.

Our findings bring first evidence of the onset of nonlinear effects in AFM spintronic devices and thus demonstrate that spin-rectification effects in AFMs with non-compensated spin dynamics as canted antiferromagnets and altermagnets will unlock unexplored nonlinear AFM dynamics by integrating efficient excitation and detection mechanisms with metallic electrodes. Extending these approaches to thin films could pave the way for efficient sub-THz spin detectors.

The authors acknowledge financial supports from Horizon 2020 Framework Programme of the European Commission under FET-Open grant agreement no. 964931 (TSAR), under Horizon Europe grant agreement no. 101070287 (SWAN) and under the ITN grant agreement ID 861300 (COMRAD). O. G. acknowledges funding by the DFG Grant No. TRR 288-422213477 (project A12) and TRR 173-268565370 (projects A11 and B15).

- 
- [1] V. Baltz, A. Manchon, M. Tsoi, T. Moriyama, T. Ono, and Y. Tserkovnyak, Antiferromagnetic spintronics, *Reviews of Modern Physics* **90**, 015005 (2018), publisher: American Physical Society.
- [2] T. Kampfrath, A. Sell, G. Klatt, A. Pashkin, S. Mährlein, T. Dekorsy, M. Wolf, M. Fiebig, A. Leitenstorfer, and R. Huber, Coherent terahertz control of antiferromagnetic spin waves, *Nature Photonics* **5**, 31 (2011), publisher: Nature Publishing Group.
- [3] E. Rongione, O. Gueckstock, M. Mattern, O. Gomonay, H. Meer, C. Schmitt, R. Ramos, T. Kikkawa, M. Micica, E. Saitoh, J. Sinova, H. Jaffres, J. Mangeney, S. T. B. Goennenwein, S. Geprags, T. Kampfrath, M. Klau, M. Bargheer, T. S. Seifert, S. Dhillon, and R. Lebrun, Emission of coherent THz magnons in an antiferromagnetic insulator triggered by ultrafast spin-phonon interactions, *Nature Communications* **14**, 1818 (2023), publisher: Nature Publishing Group.
- [4] A. V. Kimel, B. A. Ivanov, R. V. Pisarev, P. A. Usachev, A. Kirilyuk, and T. Rasing, Inertia-driven spin switching in antiferromagnets, *Nature Physics* **5**, 727 (2009), publisher: Nature Publishing Group.
- [5] Å. Johansen and A. Brataas, Spin pumping and inverse spin Hall voltages from dynamical antiferromagnets, *Physical Review B* **95**, 220408 (2017), publisher: American Physical Society.
- [6] A. Kamra, E. Thingstad, G. Rastelli, R. A. Duine, A. Brataas, W. Belzig, and A. SudbÅ, Antiferromagnetic magnons as highly squeezed Fock states underlying quantum correlations, *Physical Review B* **100**, 174407 (2019), publisher: American Physical Society.
- [7] R. A. Leenders, D. Afanasiev, A. V. Kimel, and R. V. Mikhaylovskiy, Canted spin order as a platform for ultrafast conversion of magnons, *Nature* **630**, 335 (2024), publisher: Nature Publishing Group.
- [8] S. Takei, B. I. Halperin, A. Yacoby, and Y. Tserkovnyak, Superfluid spin transport through antiferromagnetic insulators, *Physical Review B* **90**, 094408 (2014), publisher: American Physical Society.
- [9] L. Å mejkal, J. Sinova, and T. Jungwirth, Emerging Research Landscape of Altermagnetism, *Physical Review X* **12**, 040501 (2022), publisher: American Physical Society.
- [10] O. Gomonay, V. P. Kravchuk, R. Jaeschke-Ubiergo, K. V. Yershov, T. Jungwirth, L. Å mejkal, J. v. d. Brink, and J. Sinova, Structure, control, and dynamics of altermagnetic textures, *npj Spintronics* **2**, 1 (2024), publisher: Nature Publishing Group.
- [11] P. R. Elliston and G. J. Troup, Some antiferromagnetic resonance measurements in  $\hat{I}\pm$ -Fe<sub>2</sub>O<sub>3</sub>, *Journal of Physics C: Solid State Physics* **1**, 169 (1968).
- [12] A. El Kanj, O. Gomonay, I. Boventer, P. Bortolotti, V. Cros, A. Anane, and R. Lebrun, Antiferromagnetic magnon spintronic based on nonreciprocal and non-degenerated ultra-fast spin-waves in the canted antiferromagnet  $\hat{I}\pm$ -Fe<sub>2</sub>O<sub>3</sub>, *Science Advances* **9**, eadh1601 (2023), publisher: American Association for the Advancement of Science.
- [13] M. Hamdi, F. Posva, and D. Grundler, Spin wave dispersion of ultra-low damping hematite alpha-fe<sub>2</sub>o<sub>3</sub> at GHz frequencies, *Physical Review Materials* **7**, 054407 (2023), publisher: American Physical Society.
- [14] H. Wang, R. Yuan, Y. Zhou, Y. Zhang, J. Chen, S. Liu, H. Jia, D. Yu, J.-P. Ansermet, C. Song, and H. Yu, Long-Distance Coherent Propagation of High-Velocity Antiferromagnetic Spin Waves, *Physical Review Letters* **130**, 096701 (2023), publisher: American Physical Society.
- [15] Y. Mukai, H. Hirori, T. Yamamoto, H. Kageyama, and K. Tanaka, Nonlinear magnetization dynamics of antiferromagnetic spin resonance induced by intense terahertz magnetic field, *New Journal of Physics* **18**, 013045 (2016).
- [16] D. Yang, T. Kim, K. Lee, C. Xu, Y. Liu, F. Wang, S. Zhao, D. Kumar, and H. Yang, Spin-orbit torque manipulation of sub-terahertz magnons in antiferromagnetic  $\hat{I}\pm$ -Fe<sub>2</sub>O<sub>3</sub>, *Nature Communications* **15**, 4046 (2024), publisher: Nature Publishing Group.

- [17] D. Bossini, M. Pancaldi, L. Soumah, M. Basini, F. Mertens, M. Cinchetti, T. Satoh, O. Gomonay, and S. Bonetti, Ultrafast Amplification and Nonlinear Magnetoelastic Coupling of Coherent Magnon Modes in an Antiferromagnet, *Physical Review Letters* **127**, 077202 (2021), publisher: American Physical Society.
- [18] R. Cheng, J. Xiao, Q. Niu, and A. Brataas, Spin Pumping and Spin-Transfer Torques in Antiferromagnets, *Physical Review Letters* **113**, 057601 (2014), publisher: American Physical Society.
- [19] R. Cheng, D. Xiao, and A. Brataas, Terahertz Antiferromagnetic Spin Hall Nano-Oscillator, *Physical Review Letters* **116**, 207603 (2016), publisher: American Physical Society.
- [20] R. Khymyn, V. Tiberkevich, and A. Slavin, Antiferromagnetic spin current rectifier, *AIP Advances* **7**, 055931 (2017).
- [21] T. Chiba, G. E. Bauer, and S. Takahashi, Current-Induced Spin-Torque Resonance of Magnetic Insulators, *Physical Review Applied* **2**, 034003 (2014), publisher: American Physical Society.
- [22] M. B. Jungfleisch, J. Ding, W. Zhang, W. Jiang, J. E. Pearson, V. Novosad, and A. Hoffmann, Insulating Nanomagnets Driven by Spin Torque, *Nano Letters* **17**, 8 (2017), publisher: American Chemical Society.
- [23] M. Jungfleisch, W. Zhang, J. Sklenar, J. Ding, W. Jiang, H. Chang, F. Fradin, J. Pearson, J. Ketterson, V. Novosad, M. Wu, and A. Hoffmann, Large Spin-Wave Bullet in a Ferrimagnetic Insulator Driven by the Spin Hall Effect, *Physical Review Letters* **116**, 057601 (2016).
- [24] Y. S. Gui, N. Mecking, A. Wirthmann, L. H. Bai, and C.-M. Hu, Electrical detection of the ferromagnetic resonance: Spin-rectification versus bolometric effect, *Applied Physics Letters* **91**, 082503 (2007).
- [25] Å. Johansen, H. Skarsvåg, and A. Brataas, Spin-transfer antiferromagnetic resonance, *Physical Review B* **97**, 054423 (2018), publisher: American Physical Society.
- [26] Y. Zhou, T. Guo, L. Han, L. Liao, W. He, C. Wan, C. Chen, Q. Wang, L. Qiao, H. Bai, W. Zhu, Y. Zhang, R. Chen, X. Han, F. Pan, and C. Song, Spin-torque-driven antiferromagnetic resonance, *Science Advances* **10**, eadk7935 (2024), publisher: American Association for the Advancement of Science.
- [27] I. Boventer, H. Simensen, A. Anane, M. Kläui, A. Brataas, and R. Lebrun, Room-Temperature Antiferromagnetic Resonance and Inverse Spin-Hall Voltage in Canted Antiferromagnets, *Physical Review Letters* **126**, 187201 (2021), publisher: American Physical Society.
- [28] H. Wang, Y. Xiao, M. Guo, E. Lee-Wong, G. Q. Yan, R. Cheng, and C. R. Du, Spin Pumping of an Easy-Plane Antiferromagnet Enhanced by Dzyaloshinskii-Moriya Interaction, *Physical Review Letters* **127**, 117202 (2021), publisher: American Physical Society.
- [29] H. Suhl, The theory of ferromagnetic resonance at high signal powers, *Journal of Physics and Chemistry of Solids* **1**, 209 (1957), publisher: Elsevier BV.
- [30] A. J. Heeger, Spin-Wave Instability and Premature Saturation in Antiferromagnetic Resonance, *Physical Review* **131**, 608 (1963), publisher: American Physical Society.
- [31] P. H. Cole, Antiferromagnetic spin-wave instability calculations in the flopped state, *Electronics Letters* **8**, 363 (1967).
- [32] V. I. Ozhogin, Nonlinear Dynamics of Antiferromagnets with Anisotropy of the "Easy Plane" Type, *Soviet Journal of Experimental and Theoretical Physics* **21**, 874 (1965), publisher: Springer ADS Bibcode: 1965JETP...21..874O.
- [33] J. Fischer, O. Gomonay, R. Schlitz, K. Ganzhorn, N. Vlietstra, M. Althammer, H. Huebl, M. Opel, R. Gross, S. T. B. Goennenwein, and S. GeprÄggs, Spin Hall magnetoresistance in antiferromagnet/heavy-metal heterostructures, *Physical Review B* **97**, 014417 (2018), publisher: American Physical Society.
- [34] R. Lebrun, A. Ross, O. Gomonay, S. A. Bender, L. Baldrati, F. Kronast, A. Qaiumzadeh, J. Sinova, A. Brataas, R. A. Duine, and M. Kläui, Anisotropies and magnetic phase transitions in insulating antiferromagnets determined by a Spin-Hall magnetoresistance probe, *Communications Physics* **2**, 1 (2019), publisher: Nature Publishing Group.
- [35] J. Li, C. B. Wilson, R. Cheng, M. Lohmann, M. Kavand, W. Yuan, M. Aldosary, N. Agladze, P. Wei, M. S. Sherwin, and J. Shi, Spin current from sub-terahertz-generated antiferromagnetic magnons, *Nature* **578**, 70 (2020), publisher: Nature Publishing Group.
- [36] P. Vaidya, S. A. Morley, J. van Tol, Y. Liu, R. Cheng, A. Brataas, D. Lederman, and E. del Barco, Subterahertz spin pumping from an insulating antiferromagnet, *Science* **368**, 160 (2020), publisher: American Association for the Advancement of Science.
- [37] Supplementary Material includes analytical modelling of the spin-diode response, and of the linear and nonlinear response of the spin-dynamics in canted antiferromagnets. It also includes evaluation of the generated microwave field when injecting radiofrequency current in the platinum stripe, and of the associated increase in temperature.
- [38] Y.-T. Chen, S. Takahashi, H. Nakayama, M. Althammer, S. T. B. Goennenwein, E. Saitoh, and G. E. W. Bauer, Theory of spin Hall magnetoresistance, *Physical Review B* **87**, 144411 (2013), publisher: American Physical Society.
- [39] Y. Ji, J. Miao, Y. M. Zhu, K. K. Meng, X. G. Xu, J. K. Chen, Y. Wu, and Y. Jiang, Negative spin Hall magnetoresistance in antiferromagnetic Cr2O3/Ta bilayer at low temperature region, *Applied Physics Letters* **112**, 232404 (2018).
- [40] M. Althammer, S. Meyer, H. Nakayama, M. Schreier, S. Altmannshofer, M. Weiler, H. Huebl, S. GeprÄggs, M. Opel, R. Gross, D. Meier, C. Klewe, T. Kuschel, J.-M. Schmalhorst, G. Reiss, L. Shen, A. Gupta, Y.-T. Chen, G. E. W. Bauer, E. Saitoh, and S. T. B. Goennenwein, Quantitative study of the spin Hall magnetoresistance in ferromagnetic insulator/normal metal hybrids, *Physical Review B* **87**, 224401 (2013), publisher: American Physical Society.
- [41] H. Nakayama, M. Althammer, Y.-T. Chen, K. Uchida, Y. Kajiwara, D. Kikuchi, T. Ohtani, S. GeprÄggs, M. Opel, S. Takahashi, R. Gross, G. E. W. Bauer, S. T. B. Goennenwein, and E. Saitoh, Spin Hall Magnetoresistance Induced by a Nonequilibrium Proximity Effect, *Physical Review Letters* **110**, 206601 (2013), publisher: American Physical Society.